Journal of Materials Research and Technology 30 (2024) 6404–6417

Contents lists available at ScienceDirect

Journal of Materials Research and Technology

journal homepage: www.elsevier.com/locate/jmrt

"Fabrication of cutting inserts with chromium-molybdenum steel for turning operations using material extrusion technology"

Óscar Rodríguez-Alabanda [a], Guillermo Guerrero-Vacas [a,*], María Jesús Martín-Sánchez [b], Francisco de Sales Martín-Fernández [b]

[a] Department of Mechanical Engineering, Higher Polytechnic School, University of Córdoba, Rabanales University Campus, 14071, Córdoba, Spain
[b] Department of Civil, Materials and Manufacturing Engineering, School of Industrial Engineering, University of Málaga, 29071, Málaga, Spain

ARTICLE INFO

Handling editor:L Murr

Keywords:
Cutting inserts
Material extrusion
FFF technology
Metal 3d printing
Tool wear

ABSTRACT

In this study, cutting inserts for turning were produced using metal 3D printing's material extrusion technology. The primary focus was on optimizing cutting parameters. An experimental plan was devised involving rounds of cutting tests based on a design of experiments and analysis of variance. Inserts were manufactured by printing bound metal powder filament, a combination of chromium-molybdenum tool steel with a polymeric binder. After printing, green parts underwent debinding to eliminate the binder, eventually resulting in full metal parts via sintering. These inserts underwent machining tests on aluminum-copper EN AW-2030 alloy specimens. Results indicated that the inserts could function within cutting speeds (V_c) ranging from 40 to 260 m/min, feed rates (f) from 0.05 to 0.25 mm/r, and radial pass depths (a_p) from 0.1 to 2.4 mm. Optimal technological conditions were determined as $V_c = 160–200$ m/min, $f = 0.20–0.25$ mm/r, and $a_p = 1.2$ mm. Analysis revealed that cutting speed was less significant than feed rate or depth of cut on tool wear. Feed rate minimized wear within the 0.15–0.25 mm/r range, while pass depth proved most influential on wear, with optimal values between 0.8 and 1.2 mm. Surface finish, assessed through mean roughness Ra, showed high dependence on pass depth, improving for low a_p values and relatively high V_c values. These findings demonstrate that inserts fabricated via material extrusion can operate within a technological range like commercial inserts, presenting an advanced approach for customizing design and manufacturing while surpassing conventional insert limitations.

1. Introduction

Machining processes constitute a significant part of modern manufacturing, being their prevalence attributable to the high reliability, productivity and dimensional precision they offer [1]. The continued success of this industry has been based on the constant evolution of materials, geometries, machining strategies and their high automation. Manufacturing by chip removal has allowed the efficient execution of all types of parts in a wide range of materials, both those that are easy to machine and the most challenging. This level of versatility is essential to address the challenges posed by advanced designs and emerging manufacturing methodologies in the industry. Furthermore, machining techniques are very dynamic and adapts quickly to current scientific advances. In this way, we find developments with artificial intelligence, for example, to apply optimization algorithms in the adjustments of cutting parameters [2], to predict tool wear [3], or to predetermine the surface finish [4]. There is also work on digital twins to determine the life of tools [5], machine learning jobs to determine machining parameters [6] or about intelligent and sustainable machining [7]. All these works propose methodologies focused on optimizing the performance and life of cutting tools.

In this context, additive manufacturing (AM), and especially on metal alloys, is an emerging technology that has the potential to adapt to the needs for immediacy, specificity and ubiquity and can accompany and evolve the current machining manufacturing industry. Additive manufacturing makes it possible to manufacture complex parts with customized geometries and could offer remarkable advantages over other conventional processes used in the manufacturing of cutting tools. Thus, the literature shows progress in various areas. For example, tungsten carbide cutting tools have been manufactured with internal cooling channels by selective laser melting (SLM) [8]. Another contribution has consisted of laser additive manufacturing of coatings based on Ni powders dispersed with particles of MoS_2 y Al_2O_3 that self-lubricate the cutting tool [9]. Other consulted work has made it

* Corresponding author.
E-mail address: guillermo.guerrero@uco.es (G. Guerrero-Vacas).

https://doi.org/10.1016/j.jmrt.2024.05.065
Received 11 March 2024; Received in revised form 7 May 2024; Accepted 7 May 2024
Available online 8 May 2024

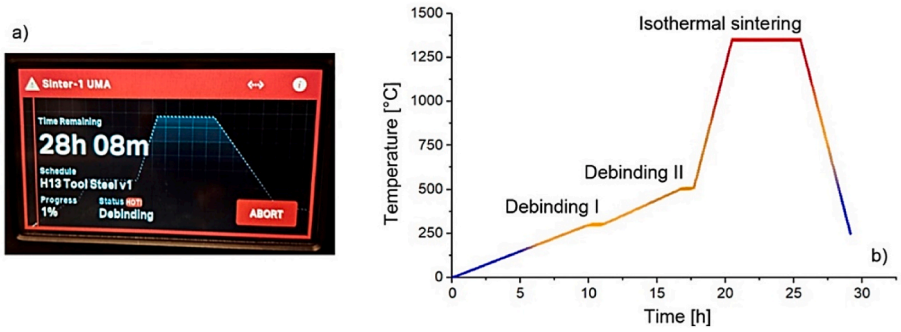

Fig. 1. Sintering conditions: a) Markforged Sinter-1 screen, b) debinding-sintering cycle for AISI H13 steel from Li et al. [22].

possible to manufacture inserts similar to the commercial ones, but made of martensitic steel X3NiCoMoTi 18-9-5 also by SLM, allowing to obtain dimensional and surface quality of the same order as conventional ones [10]. Also, in another work Stellite™ (Co–Cr–W superalloy) multilayer structures were deposited on stainless steel with the LENS technique (Laser Engineered Net Shaping) and, after cutting this material, the tool obtained could be used for applications of high resistance and ductility [11]. Finally, faced with the dare of manufacturing a carbide tool directly through additive manufacturing, various AM techniques have been studied such as SLM, SEBM (Selective Electron Beam Melting), BJAM (Binder Jet Additive Manufacturing), 3DGP (3D Gel-Printing) and FFF (Fused Filament Fabrication) and the challenges and limits of each of them have been debated [12]. Along the same lines, working with carbide tools reinforced with diamond using the direct energy deposition technique (DED) has allowed to significantly improve some properties with respect to conventional inserts [13].

The application of the material extrusion, commonly referred as fused filament fabrication (FFF) technique in the present work stands out for its remarkable efficiency in minimizing manufacturing costs, significantly outperforming powder bed metal 3D printing systems. Additionally, this methodology eliminates complex dust management, and the requirement for personal protective equipment is considerably less compared to laser-based systems [14].

In this study, we have selected high speed tool steel AISI H13 [15,16] as the main metal material for the manufacture of cutting inserts for turning. This type of steel has been widely investigated in various aspects related to machining processes. For example, previous studies [17] have examined their impact on cutting forces during milling operations, while additional research [18] have explored the influence of the temperature of the tempering treatment on its microstructure. Other authors have addressed the study of its mechanical properties according to processing conditions [19]. In addition, a predictive model of cutting temperatures has been developed [20] specifically for this material. The roughness resulting from additive manufacturing processes on H13 steel has also been the subject of analysis [21], as well as the post-processing effect in metal alloys manufactured through additive manufacturing [22].

On the other hand, it is vitally important to study the viability and efficiency of these new cutting tools. To do this, a robust methodology must be developed that allows evaluating the optimal technological conditions of machining and the life of the tool. Among the various ways to approach it are studies through the Taguchi method. There are many examples of application of this method in the analysis and optimization of these type of processes. For example for machining steels [23,24], for pearlitic casting GG25 [25] or for aluminum alloys [26,27].

In short, given the constant evolution in additive manufacturing and the challenges of modern manufacturing, it is of great interest to develop and deepen proposals for the creation of new generation cutting tools and study their advantages and influence on the machining process. In this research, a set of cutting inserts has been manufactured with a special chromium-molybdenum high speed tool steel AISI H-13 with a standardized DCMT 11T308 geometry [28] using material extrusion technology. The cutting speed (V_c), feedrate (f) and pass depth (a_p) in turning operations of an aluminum-copper alloy EN AW-2030 [29,30] have been evaluated through a design of experiments (DoE) based on the Taguchi method. The surface quality of the machined parts has also been addressed and a study on tool wear has been carried out.

2. Materials y methods

2.1. Additive manufacturing of the cutting inserts

The cutting inserts have been manufactured with the Markforged Metal X™ System additive manufacturing equipment. The technology used is called ADAM (Atomic Diffusion Additive Manufacturing). According to the ISO/ASTM classification, this technology would be recognized as a material extrusion technique. The extruded filament is composed of metal powder compacted with a polymeric binder, and this is the material used to shape the cutting inserts. A secondary filament, composed of ceramic material, acts as a separating element between the part and the support/raft material, if necessary, and thus facilitate the support/raft removal after sintering.

For manufacturing, first, the insert is modeled according to the standardized shape and dimensions, using Solidworks CAD software (Dassault Systèmes, Paris, France) and exported in STL format to Markforged Eiger slicing software (Markforged, Watertown, Massachusetts, USA). For printing, a horizontal orientation of the insert was chosen, avoiding supports or possible distortions that could occur if a vertical orientation was chosen. Twelve parts have been printed simultaneously.

After printing, the parts must be washed in the Markforged Wash-1 equipment to eliminate the polymeric binder. This debinding step removes almost all the binding material by dissolving it into a heated solvent bath with Opteon SF-79 key solvent at 115 °C (The Chemours Company CC, LLC. Wilmington, Delaware, USA). When the green parts have loss more than 4.2% of mass, they pass to the drying chamber (brown parts) before the sintering process in the Markforged Sinter-1 furnace to eliminate the rest of the binding material and consolidate the metallic base material. Although the sintering data of the equipment is confidential from the supplier, a previous work [22] defined the ideal debindering-sintering cycle compatible with a composite matrix of H13 steel powder with polymeric binder, determining a temperature range of 283 °C–460 °C compatible with the decomposition of all type of polymeric binder. The sintering temperature for AISI H13 steel has been experimentally stablished at 1350 °C, just 100 °C below its melting point ($T_{melting\ (AISI\ H13)} \approx 1450$ °C). Thus, they designed a post-processing cycle with heating ramps by 0.5 °C/min to get two debinding points (300 °C during 1h and 500 °C during 1h), and then increasing by 5 °C/min until reaching sintering temperature, maintaining it for 5 h. Finally, they recommend a cooling ramp to 250 °C by 5 °C/min followed by cooling to room temperature outside the sinter (Fig. 1). This information involves a complete cycle of approximately 29 h, compatible

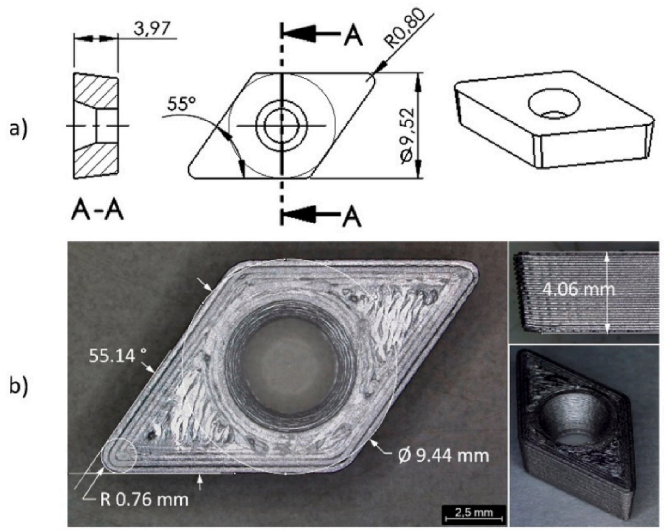

Fig. 2. Standard dimensions of the DCMT 11T308 insert inn mm (a), insert manufactured by FFF (b).

with the time observed on the screen of the Sinter-1 used in this work. The sintering chamber is protected by argon + argon-hydrogen mix gases, Alphagaz 1 argon and 3D Heat mix 2.9% H_2 (Air liquid España, S. A., Madrid, Spain), to avoid metal oxidation.

The inserts have been manufactured with the geometry equivalent to a commercial rhombic-shaped insert with a tip angle of 55°, designed as DCMT 11T308. Fig. 2 shows the theoretical values of the normalized dimensions for this designation, as well as a series of images showing the final appearance of the manufactured insert and its actual dimensions. The geometry and dimensions of the manufactured inserts has been checked on the Leica DVM6 digital microscope (Leica, Wetzlar, Germany), and it has been verified that they meet the tolerances indicated in the ISO 1832:2017 [28].

The printing position has been decided after three printing tests in different orientations of the insert: resting on its lower face (Fig. 3a), resting on one of the side faces (Fig. 3b) and resting in a vertical position or on one of the tips (Fig. 3c). In addition, it should be noted that vertical positions (Fig. 3b and c) have required to include raft and, to a lesser or greater extent, the addition of support material.

The images in Fig. 3d, e and 3f show the geometric quality obtained in the main cutting edges and at the tip of the inserts, in each of the three orientations that made manufacturing possible. As it can be clearly seen, the insert manufactured according to the orientation of Fig. 3e, resting on a lateral face, has slight defects on two of the four cutting edges and an ill-defined tip radius. The insert manufactured in the orientation of Fig. 3f, resting on one of its tips, presents a very poor geometric definition in the tip radius. However, the insert manufactured in the orientation of Fig. 3d, resting on the lower face, presents the best quality in the main cutting edges and in the geometry of the tip radius. Furthermore, it can be seen how in this case the deposition of layers is carried out perpendicular to the action of the shear stress that will act on the upper face of the insert. Consequently, this orientation has been selected to manufacture all the inserts necessary for the experiments.

The technical specifications of the printing process are indicated on Table 1.

2.2. Materials for the inserts and part specimens

Fifty-four inserts have been manufactured via metal additive manufacturing and the experimental rounds have been defined in Table 2 as rounds A to E. Nine additional inserts were also printed for dimensional control and characterization purposes.

Table 1
Printing settings (left) and output data as a function of printing orientation (right).

Printing parameters	Settings	Orientation	Raft	Printing time	Material (cm^3)	Cost (USD)
Layer height	0.125 mm	horizontal	NO	1h 24 m	0.52	0.60
Fill pattern	Solid	vertical (side)	YES	1h 56 m	1.84	2.13
External wall layers	4	vertical (tip)	YES	2h 02 m	1.50	1.73

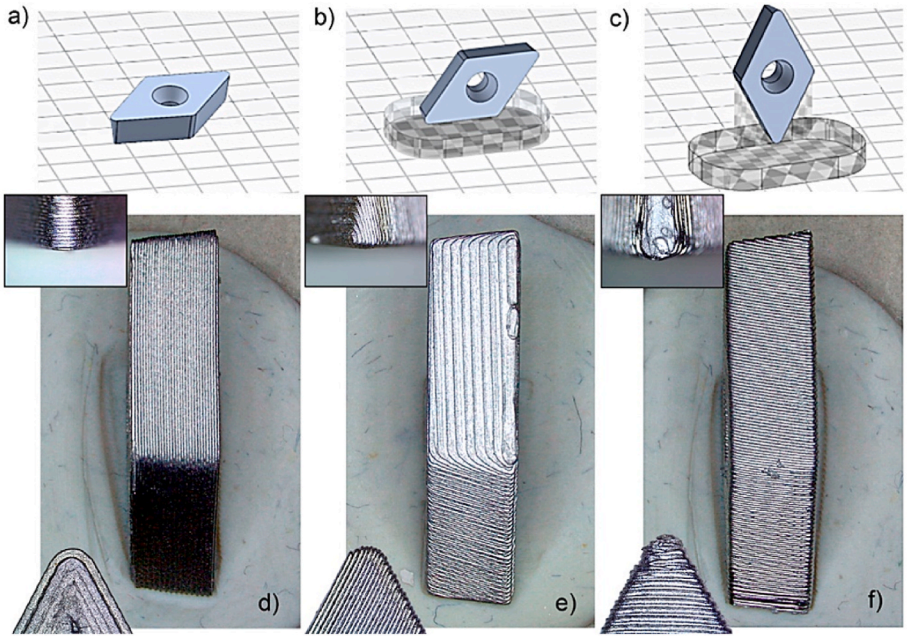

Fig. 3. Printing orientations and its influence on the insert quality: a), d) resting on the lower face (horizontal), b), e) resting on one side face (vertical), c), f) resting on the tip (vertical).

Table 2
General organization of the experiments, identification and number of inserts used.

Test rounds	Identification	Nr. of inserts
Control and characterization	1…….9	9
Round A	A1 to A9	9
Round B	B1 to B9	9
Round C	C1 to C9	9
Round D	D1 to D9	9
Round E	E1 to E9	9

The material used for the additive manufacturing of the cutting inserts was the AISI H13 tool steel (X40CrMoV5-1) from the manufacturer Markforged (Markforged, Watertown, Massachusetts, USA). Tool steel AISI H13 [15] is an appropriate material for working tools and dies in the forging and die casting industry [31] and it offers a good compromise between hardness and fracture resistance at high temperatures, as well as good resistance to abrasion wear. The steel is supplied in filament format (metal powder and polymeric binder) by Markforged, and it has been used according to the protocol proposed by the supplier of the printing equipment used.

The sintered material in the form of an insert has shown a mean value of Rockwell hardness 40.7 HRC, according to the EN-ISO standard [32]. The hardness measurement has been done on a ZHU-250 top model equipment, from the Zwick-Roell brand (Zwick-Roell, S. L., Sant Cugat del Vallés, Barcelona, Spain), using a conical diamond indenter, according to the indicated procedure and reiterating the measurement three times on three of the manufactured inserts. Table 3 shows the composition data of the manufactured inserts, which have been determined by SEM-EDX (Scanning Electron Microscopy - Energy Dispersive X-ray spectroscopy) in the field emission scanning electron microscope JEOL JSM 7800F (JEO Ltd., Tokyo, Japan).

The SEM-EDX analysis of the main alloying elements of the H13 steel filament used for the AM of the inserts has shown values that are in accordance with the those indicated in the ASTM standard [15], as shown in the EDX spectrum of Fig. 4 (left). The images in Fig. 4 (right) show the surface quality, texture and porosity of the material once sintered, observing surface pores between 5 and 10 μm.

Aluminum-copper alloy EN AW-2030 [29,30], in the form of cylindrical bars Ø 80 × 120 mm length supplied by Broncesval (Broncesval S. L, Valencia, Spain), has been used for the turned specimens. This aluminum alloy has excellent machinability and good chip release. The machining operations have been carried out using 6% water emulsifiable cutting fluid Servol 550 (Brugarolas, S.A., Barcelona, Spain), specifically formulated for high severity machining and compatible with machining steel, aluminum, and brass alloys. Fig. 5 shows the dimensions of the machined specimens.

In the rounds corresponding to the sensitivity tests (36 tests in four rounds A-B-C-D), the turning cycle consisted of a roughing turning operation over a length of 80 mm, from an initial diameter of 38 mm to a final diameter of 33.2 mm, and a final finishing pass. In the final round (round E), a length of 80 mm was roughed, from an initial diameter of 80 mm to a final diameter of 20 mm, with a final finishing pass. In all cases the operation has been carried out with lubricant-refrigerant action.

The machining equipment used is a CNC lathe model TB-46 M from CMZ (CMZ Machinery Group SA, Vizcaya, Spain) with 14 kW of power and up to 5000 rpm, which is equipped with a numerical control unit from the manufacturer Fanuc, model 32i (Fanuc Ltd. , Oshino-mura, Yamanashi Prefecture, Japan). The CNC–ISO [33] programs have been developed with Solidworks CAM software (Dassault Systèmes, Paris, France).

2.3. Design of experiments and statistical analysis of the results

For the design of experiments (DoE) and the statistical analysis of the results, the Minitab software (Minitab, Inc., Pennsylvania, USA) was used. Thus, Taguchi method has been implemented selecting a L9 orthogonal array, in all 4 successive rounds of testing (36 experiments) to determine the sensitivity about the factors involved in the analysis. Then, a final round to study the tool wear and life has been designed by the same way (9 experiments). Minitab has made it possible to analyze

Table 3
Composition (%) by weight of AISI H13 normalized steel powder and inserts obtained by additive manufacturing according to EDX analysis.

Material	Si	Mn	Cr	Mo	V	C	Fe
AISI H13 (standard)	0.80–1.20	0.20–0.50	4.75–5.50	1.10–1.75	0.80–1.20	0.3–0.45	bal.
AISI H13 (SEM-EDX analysis)	1.08	0.52	5.16	1.65	1.205	–	bal.

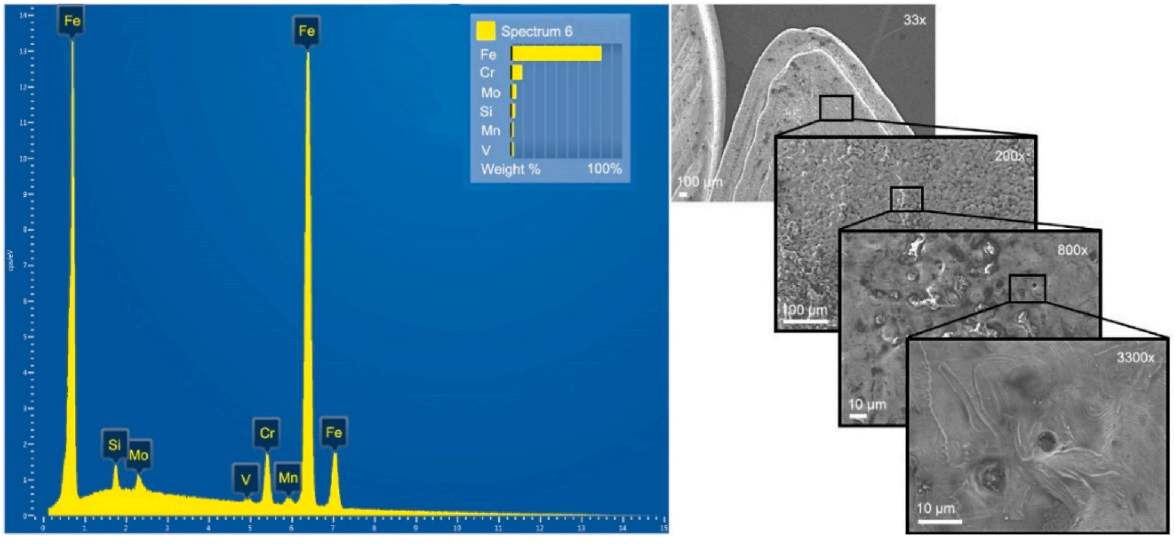

Fig. 4. EDX spectrum of the processed material in the form of an insert (left) and surface appearance of the manufactured insert (right).

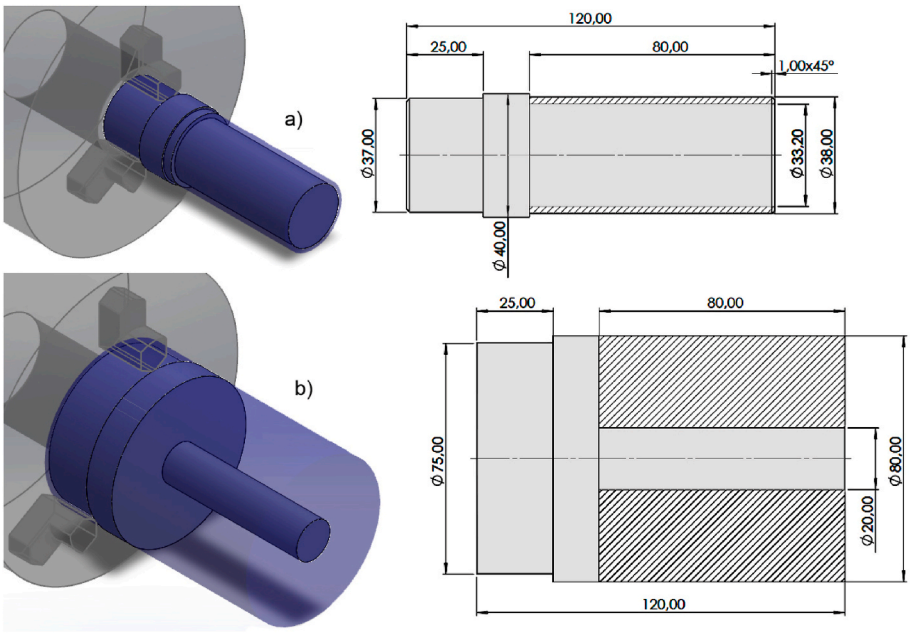

Fig. 5. Dimensions in the turned aluminum specimens (mm): a) ABCD test rounds, b) E test round.

Table 4
Technological conditions of the different rounds of experimental testing.

Round	Removed vol. [mm^3]	V_c [m/min]	f [mm/r]	a_p [mm]
Round A	20131.33	40, 60, 80	0.05, 0.10, 0.15	0.4, 0.8, 1.2
Round B	20131.33	40, 60, 80	0.10, 0.20, 0.30	0.4, 0.8, 1.2
Round C	20131.33	40, 60, 80	0.10, 0.20, 0.30	0.8, 1.6, 2.4
Round D	20131.33	80, 120, 160	0.10, 0.20, 0.30	0.8, 1.6, 2.4
Round E	376991.12	160, 200, 220	0.15, 0.20, 0.25	0.6, 0.9, 1.2

the influence of the machining parameters V_c, f and a_p as the main technological factors affecting tool wear and life.

Since after the first round A (9 runs) the inserts did not show any signs of wear, a second round B was carried out in which the feedrate (f) was doubled to subject the inserts to greater stress. In a third round C, the values of the pass depth (a_p) were also doubled. As the inserts still did not show significant signs of wear, despite finding discolorations due to the high working temperatures, the value in the cutting speed (V_c) was also doubled, carrying out a fourth round D to complete a total of 36 runs determining the sensitivity of the experiment to these factors. Definitively and based on these preliminary results, the need to increase the work cycle time was determined, thus eliminating a greater volume of material to better assess the evolution of wear on the main cutting edge of the insert. So, a final round of experiments (round E) was designed to properly evaluate the tool wear and life (round E). Table 4 details the working conditions established for the different experimental rounds.

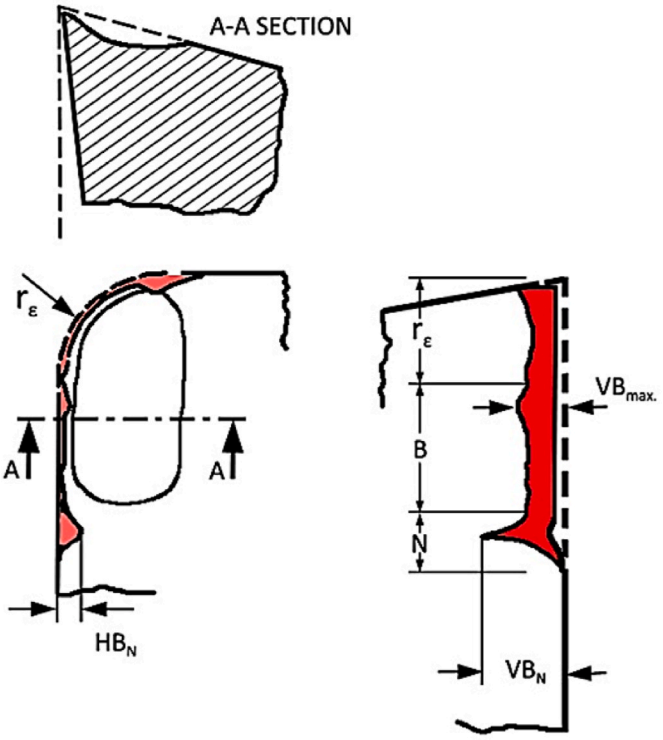

Fig. 6. Detail of the wear parameters on the cutting tool: r_ε, tool tip radius; HB_N, notch wear depth; VB_N, notch wear height; VB_{max} maximum flank wear; B, flank wear zone; N, notch wear zone.

2.4. Characterization

2.4.1. Surface analysis of the machined specimens

A Mitutoyo SJ-201 roughness tester (Mitutoyo Corporation, Kakatsuku, Kawasaki, Kanagawa, Japan) was used to obtain the linear roughness on the surfaces of the machined specimens. The mean roughness (Ra) is the average distance between the peaks and valleys and the deviation from the mean line on the entire surface within the sampling length and the absolute peak to valley average of five sequential sampling lengths within the measuring length is Rz [34]. The values of these roughness parameters were obtained after repeating the measurement five times in three cylinder generatrix on each machined specimen.

2.4.2. Analysis of the wear of the main cutting edge of the insert

For the analysis of wear in the main cutting edge of the tool, plant

Table 5
Input variables and results corresponding to preliminary round A.

Run	V_c [m/min]	**f [mm/r]**	a_p [mm]	Ra [μm]	**Rz [μm]**	H_{BUE} [μm]	**t [s]**
A1	40	0.05	0.4	0.33	2.76	438.37	1687
A2	40	0.10	0.8	2.88	13.67	0.00	420
A3	40	0.15	1.2	4.27	21.61	585.20	432
A4	60	0.05	0.8	1.27	8.21	0.00	566
A5	60	0.10	1.2	5.50	26.94	571.61	235
A6	60	0.15	0.4	6.33	25.07	545.60	420
A7	80	0.05	1.2	2.64	13.20	0.00	309
A8	80	0.10	0.4	4.39	20.41	491.01	440
A9	80	0.15	0.8	4.25	21.23	556.93	193

and profile view images of the inserts were obtained on the Leica DVM6 digital microscope and analyzed with Leica LAS X software (Leica Microsystems, L'Hospitalet de Llobregat, Spain). After each test, the value of the wear parameters defined in Fig. 6 has been measured: the notch wear depth (HB_N) and the notch height on the flank (VB_N). The maximum wear value on the main cutting edge (VBmax) was not measured due to the aluminum welded/added to the edge in the cutting operation.

2.4.3. Metallographic testing

A metallographic study was carried out on the insert's representative of the various phases of the research. The inserts have been encapsulated in resin oriented in the area of interest and polished in different stages to colloidal silica abrasives. The images were obtained with the Leica CTR 6500 metallographic microscope (Leica Microsystems, L'Hospitalet de Llobregat, Spain).

The samples were etched for 3 min with an acid solution composed of glycerol, nitric acid and hydrochloric acid in a volume ratio of 3:1:2, respectively.

3. Results

3.1. Preliminary tests of sensitivity to experimental factors

Initially, based on the lack of knowledge of the cutting capacity of the manufactured insert and its durability, a preliminary experiment plan has been designed to undertake a sensitivity study that would approximate to the working limit conditions of the insert on the aluminum alloy object of study.

In a first round A of preliminary tests, in which nine experiments were established according to Taguchi L-9 design, the values of the input variables were set according to Table 4 indicated above. Table 5 shows the results of these tests and the responses obtained, on the one hand, surface roughness parameters (Ra, Rz), height of the built-in edge (H_{BUE}) and, finally, the roughing cycle time (t).

The images in Fig. 7 show the state of the cutting edge after tests A7, A8 and A9. In these images it can be seen that in none of the cases the main cutting edge has suffered any significative damage and only differences have been seen in terms of the built-in edge (H_{BUE}) phenomenon. It must be considered that the roughing cycle with turning passes parallel to the axis of rotation ends with a cylindrical finishing pass including face turning of flat surfaces and the built-in edge easily detaches from the edge again.

It has been verified that, in all 9 cases, the built-in edge (H_{BUE}, adhered material) easily detaches from the edge, leaving it practically intact. From this result it can be deduced that the working conditions are not at all aggressive, if we consider the volume of material removed during the tests and the working time in each of them. Thus, it was decided to carry out a second round B of tests doubling the values in the range of the feedrate (f) in the programmed rough cylindrical turning passes. The results of round B of experiments are presented in Table 6.

The images in Fig. 8 show the state of the main cutting edge once the turning and finishing cycles corresponding to tests B7, B8 and B9 have finished.

The cutting edge still does not suffer any significant damage, although there is a greater accumulation of welded material, longer and higher for a higher feedrate and a medium value depth of pass. Consequently, it was decided to undertake a third round C, also doubling the pass depth (a_p) in the roughing cycle. The results of round C are shown in Table 7.

Fig. 9 shows the state of the main cutting edge once the roughing/finishing cycle corresponding to tests C7, C8 and C9, which are those carried out with more aggressive conditions than those in round A and B.

Once again, it can be seen that, for the volume of material removed and with the established working conditions, the inserts have supported perfectly without noticeable deformations or breaks in the main cutting edge. However, a notable increase in the height of the built-in edge (H_{BUE}) has been observed, anchored more firmly. This fact may be due to the supposed increase in localized temperature, which causes the cut material to weld more easily and strongly to the cutting edge during the final finishing and facing pass. Consequently, a fourth round D has been proposed in which all three technological input factors involved doubled their value with respect to those initially implemented in the initial round A. Thus, Table 8 shows the results of the fourth preliminary round D.

The images in Fig. 10 show the main cutting edge after the roughing and finishing turning cycle corresponding to run tests D7, D8 and D9.

From the results of this fourth preliminary round D, it has been

Table 6
Input variables and results corresponding to preliminary round B.

Run	V_c [m/min]	**f [mm/r]**	a_p [mm]	Ra [μm]	**Rz [μm]**	H_{BUE} [μm]	**t [s]**
B1	40	0.1	0.4	1.71	8.34	593.15	840
B2	40	0.2	0.8	8.60	41.66	596.14	216
B3	40	0.3	1.2	13.02	59.35	813.63	131
B4	60	0.1	0.8	2.21	11.39	556.66	314
B5	60	0.2	1.2	4.88	24.14	582.56	132
B6	60	0.3	0.4	9.47	43.89	749.40	240
B7	80	0.1	1.2	6.61	30.67	517.20	175
B8	80	0.2	0.4	5.95	27.90	586.12	263
B9	80	0.3	0.8	11.44	54.67	632.72	113

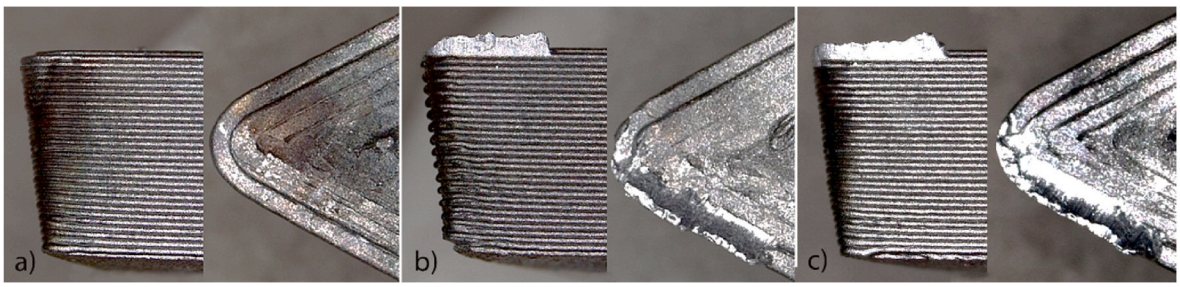

Fig. 7. Appearance of the cutting edge after the runs a) A7, b) A8 and c) A9.

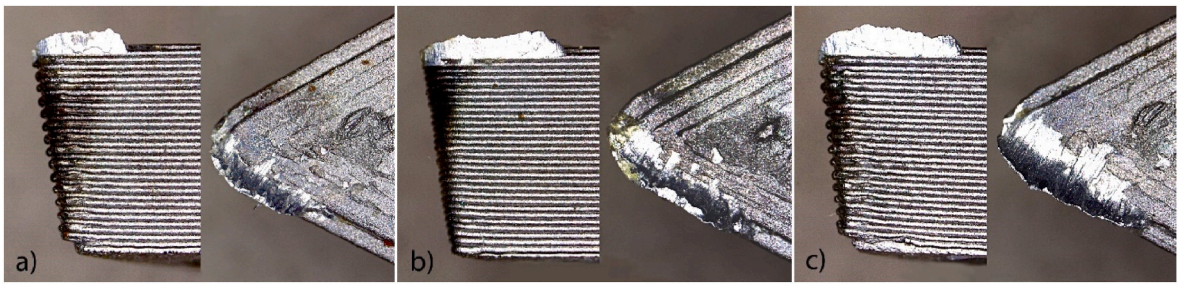

Fig. 8. Appearance of the cutting edge after the runs a) B7, b) B8 and c) B9.

Table 7
Input variables and results corresponding to preliminary round C.

Run	V_c [m/min]	**f [mm/r]**	a_p [mm]	Ra [μm]	**Rz [μm]**	H_{BUE} [μm]	**t [s]**
C1	40	0.1	0.8	5.74	26.56	144.61	783
C2	40	0.2	1.6	8.13	37.95	687.29	214
C3	40	0.3	2.4	7.54	36.78	848.46	115
C4	60	0.1	1.6	4.88	23.81	150.11	293
C5	60	0.2	2.4	8.08	38.08	720.63	122
C6	60	0.3	0.8	10.44	48.49	795.19	227
C7	80	0.1	2.4	3.42	18.07	511.22	163
C8	80	0.2	0.8	9.36	43.66	730.70	247
C9	80	0.3	1.6	7.33	35.44	753.09	108

deduced that inserts manufactured using FFF additive technology are very resistant and withstand the turning conditions without any deterioration apart from the built-in edge observed, whose size and firmness increases as the cutting conditions become more severe. Furthermore, it has been concluded that the hardest conditions linked to this fourth round D (V_c = 160 m/min, f = 0.3 mm/r, a_p = 2.4 mm) are perfectly viable to work with those additively manufactured turning inserts.

If the results of the four preliminary rounds are observed, in terms of roughness, it can be said that the average values of the mean roughness ($\overline{Ra}$) achieved after the work cycle ($\overline{Ra}_A$ = 3.54 μm, $\overline{Ra}_B$ = 7.1 μm, $\overline{Ra}_C$ = 7.21 μm, $\overline{Ra}_D$ = 5.21 μm) is better when working within the ranges established in the round A ($\overline{Ra}_A$ = 3.54 μm), combined with the lowest pass depth (a_p) and feed rate (f). Thus, it is observed that when the value of these two variables is increased without increasing the cutting speed (V_c), then the average roughness on the finished surface worsens noticeably, practically doubling its average value ($\overline{Ra}$) as observed in rounds B and C ($\overline{Ra}_B$ = 7.1 μm, $\overline{Ra}_C$ = 7.21 μm). Finally, it has been observed as the average value obtained for Ra slightly improves by increasing the range of values for the cutting speed ($\overline{Ra}_D$ = 5.21 μm).

From all these observations, it can be concluded that the conditions imposed in the fourth round of preliminary tests (round D) are closer to the optimal working conditions of the additively manufactured inserts. In this way, the highest cutting speed (V_c = 160 m/min) allows obtaining a reasonably good surface finish (with Ra values between 2.14 μm and 7.57 μm) and in a very fast cycle time, also without any deterioration in the main cutting edge of the tool. However, an important built-in edge produced mainly in the last pass of the cycle (finishing + facing) has been observed, although built-in aluminum is not tightly welded, and it has been found that it can be detached from the cutting edge relatively easily.

The results of the preliminary tests also show that, most likely, the insert is capable of working during a much longer roughing cycle than that programmed with this preliminary specimen, since the cutting edge is practically intact in all 36 runs. Thus, it has been decided to design a new specimen to design and program a roughing cycle in which a greater volume of material is removed, increasing the cycle time (t) in order to ensure that the inserts work at the limit of their capacity. In this way it will be possible to assess a better evaluation of the life of this insert for working on this aluminum alloy, determining its optimal and recommended conditions to make the most of the life of the proposed cutting tool.

3.2. Design of experiments for the evaluation of insert life

For a better evaluation of the tool life, an additional round of experiments has been proposed (round E). To define the experimental conditions, the results obtained in the preliminary sensitivity tests have been analyzed, but the manufacturer's recommendation KYOCERA has also been considered (KYOCERA Precision Tools, Hendersonville, USA). Thus, the recommended working conditions for a KYOCERA's commercial reference insert DCMT 11T308, grade KW10, for materials to be

Table 8
Input variables and results corresponding to preliminary round D.

Run	V_c [m/min]	**f [mm/r]**	a_p [mm]	Ra [μm]	**Rz [μm]**	H_{BUE} [μm]	**t [s]**
D1	80	0.1	0.8	1.49	8.35	107.06	390
D2	80	0.2	1.6	5.38	28.26	721.27	214
D3	80	0.3	2.4	6.31	32.44	753.09	82
D4	120	0.1	1.6	4.98	24.79	509.29	170
D5	120	0.2	2.4	5.88	29.27	726.81	70
D6	120	0.3	0.8	8.65	42.17	739.81	129
D7	160	0.1	2.4	2.14	12.80	628.54	71
D8	160	0.2	0.8	7.57	36.89	599.17	104
D9	160	0.3	1.6	4.50	23.54	608.37	39

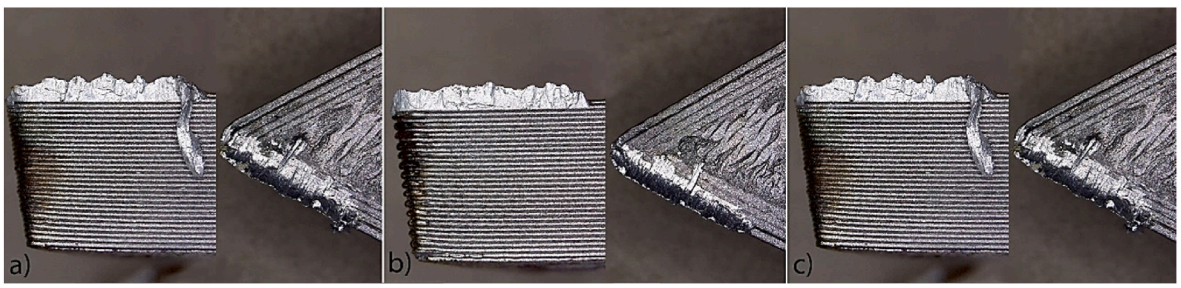

Fig. 9. Appearance of the cutting edge after the runs a) C7, b) C8 and c) C9.

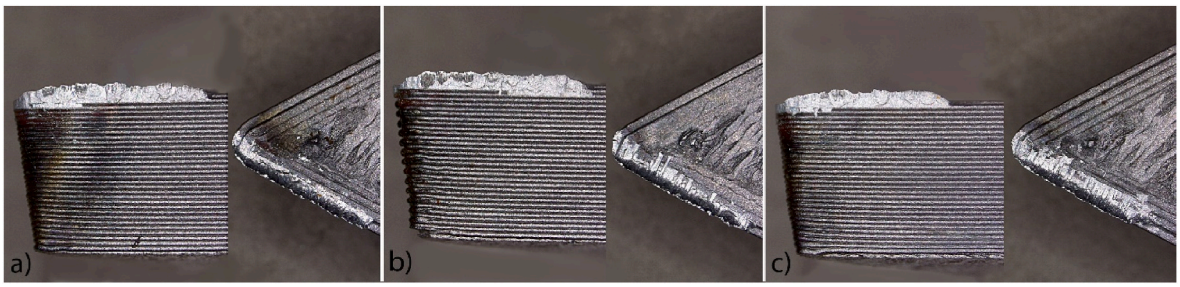

Fig. 10. Appearance of the cutting edge after the runs a) D7, b) D8 and c) D9.

Table 9
Cutting recommendations for the KYOCERA Grade KW10 insert reference DCMT 11T308, for type N materials to be machined.

Insert code	V_c [m/min]	f [mm/r]	a_p [mm]
DCMT 11T308 KW10	30–300	0.05–0.25	0.5–3

machined type N, and with geometry analogous to the one studied, but made of tungsten carbide, have been taken as a reference. In this way, ranges have been established for the technological variables or process input factors (V_c, f and a_p) so that the minimum values have been determined fundamentally by observing the results of the preliminary round D, while the maximum values have been established by observing these same preliminary results and also considering the recommendations given by the supplier for its commercial insert. The new input values are as shown in Table 9.

It should be noted that, in this case, in each of the nine tests planned in this design of experiment (DoE), regularly scheduled stops have been planned to be able to measure the progression of the established flank wear parameters (wear depth of notch on the flank, HB_N and height of notch on the flank, VB_N) as a function of the working time of the tool (t). In addition, the height of the input edge (H_{BUE}) was also measured at each stop, and also the partial machined effective diameter ($Ø_{EF.}$) to control the correction of the diameter obtained in the specimen during each test and included in Supplementary Tables S1–S9. A summary of results obtained on each experiment in the round E is shown in Table 10.

The evolution of wear parameters HB_N and VB_N, controlled during each one of these nine experiments, has been represented graphically in Figs. 11 and 14. The trend curves have been obtained by applying third-order polynomials for non-linear behaviors and second-order polynomials in the case of quasi-linear behaviors. Tables S1–S9, included in the supplementary material, present the partial results corresponding to the stopping points represented in the graphs, with the values of the evolution of the flank wear in each of the experiments of round E.

The graph in Fig. 11 shows the representative curves of the progression observed in the measured depth of the maximum wear or notch (HB_N), which is generated on the flank of the main cutting edge of the insert as the machining cycle evolves. The curves represent the trend in the evolution of wear parameter HB_N, depending on the cutting conditions applied. Initially, it is observed that, in the case of the depth of flank notch wear (HB_N) and considering a tool cutting edge life of 15 min (900 s), the conditions of the E1 run test (black color) seem that have caused less wear. However, it must be considered that this test has not yet eliminated the entire volume of material expected in 15 min, since this has required a much longer cycle than the rest of the experiments and close to 29 min (1740 s) to eliminate all the planned volume.

On the other hand, as can be seen in the images shown in Fig. 12, although the working conditions in this experiment seem to be the least demanding of the entire set (V_c = 160 m/min, f = 0.15 mm/r, a_p = 0.6 mm), these cause considerable wear in the area near the tip of the insert in the longest work cycle of all those tested (E1), consequently offering lower efficiency in the material removal rate because of a longer cycle time.

Likewise, it can be seen that the conditions of experiments E3 and E5 (light green and light blue) are the most efficient in terms of the cycle time used to eliminate the programmed volume of material and, in addition, the working conditions of E5 provoked much lower tool wear (VB_N, HB_N) than the rest of the experiments (see Table 10). The state in which the cutting edge remains after completing the full working cycle

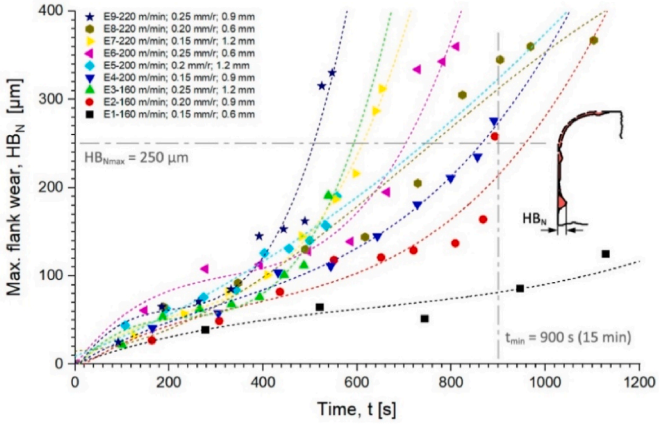

Fig. 11. Evolution of the depth of the flank notch wear (HB_N) vs. machining time for different cutting conditions.

Table 10
Summary of the results obtained in the round E.

Run	V_c [m/min]	f [mm/r]	a_p [mm]	Ra [µm]	Rz [µm]	VB_N [µm]	HB_N [µm]	H_{BUE} [µm]	time, t [s]
E1	160	0.15	0.6	4.51	28.50	2311	290.00	2678.00	1740
E2	160	0.20	0.9	4.51	27.83	1514	258.00	1759.00	893
E3	160	0.25	1.2	4.23	23.50	1036	191.00	1355.00	539
E4	200	0.15	0.9	3.45	22.24	1698	276.00	1980.00	891
E5	200	0.20	1.2	3.73	24.34	993	190.44	1158.66	557
E6	200	0.25	0.6	3.87	24.52	1875	360.46	1875.87	811
E7	220	0.15	1.2	2.47	13.87	1918	312.00	1489.00	653
E8	220	0.20	0.6	3.81	20.62	1975	367.00	1983.00	1103
E9	220	0.25	0.9	5.17	27.49	2354	330.00	920.00	547

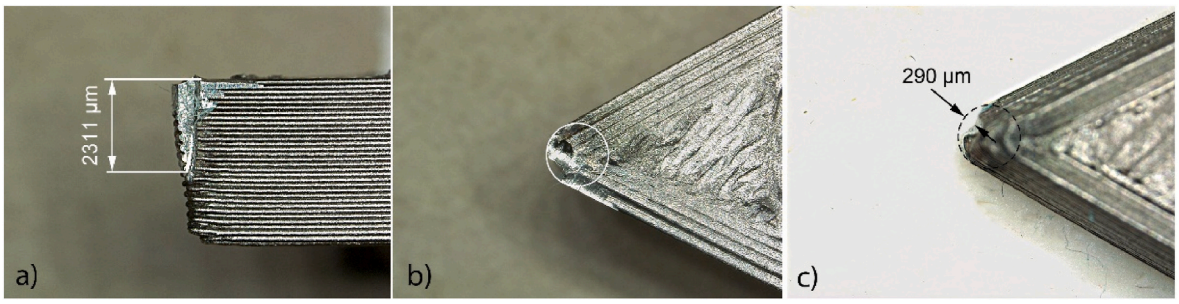

Fig. 12. Appearance of the cutting edge at the end of run E1: a) side view, b) top view, d) bottom view (V_c = 160 m/min, f = 0.15 mm/r, a_p = 0.6 mm, t = 1740 s).

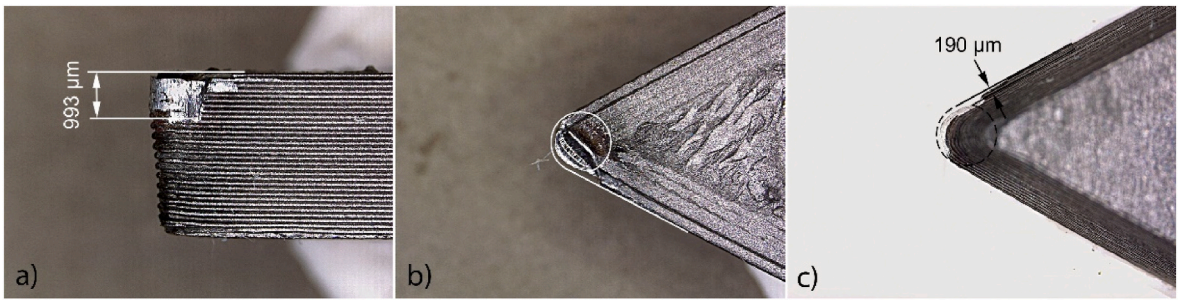

Fig. 13. Appearance of the cutting edge at the end of run E5: a) side view, b) top view, d) bottom view (V_c = 200 m/min, f = 0.20 mm/r, a_p = 1.2 mm, t = 557 s).

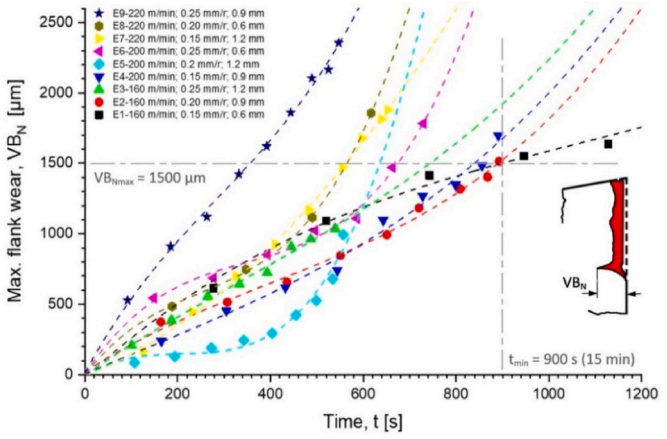

Fig. 14. Evolution of the height in the flank notch wear (VB_N) vs. machining time for different cutting conditions.

in just 557 s (a little more than 9 min) is shown in the images in Fig. 13. Thus, the working conditions of experiment E5 (V_c = 200 m/min, f = 0.20 mm/r, a_p = 1.2 mm) have allowed efficient removal of all the material from the specimen with the lower measured wear. Furthermore, experiment E3 (light green and V_c = 160 m/min, f = 0.25 mm/r, a_p = 1.2 mm) also presents a high efficiency (t = 539 s) with a reasonable wear value $HB_N \approx 200$ µm after removing all the programmed volume.

Fig. 14 shows the progression graphs corresponding to the measured height of the maximum notch wear (VB_N), generated on the flank of the main cutting edge of the insert as the working cycle evolves. The curves represent the trend in the evolution of said wear parameter (VB_N), as a function of the cutting conditions applied and time.

In these graphs, four experiments are distinguished whose trend is more prone to greater edge durability. These experiments are those corresponding to tests E1, E2, E3 and E4, which present a progressive evolution of the wear parameter VB_N during the working cycle. Longer and less efficient cycles are obtained in cases E1, E2 and E4, while experiment E3 (light green color) shows very good efficiency by eliminating the entire programmed volume in a relatively short cycle time and for a significantly lower height in the flank notch wear (VB_N) than that obtained in the rest of the experiments.

On the other hand, the conditions of experiment E5 are also very efficient, with a very short cycle time to eliminate the programmed volume of material. However, although this case has allowed a VB_N wear value, at the end of the cycle, that is noticeably lower than the rest, its trend in the VB_N wear curve (in light blue) suggests a limited durability of the insert for a longer working time in these technological conditions.

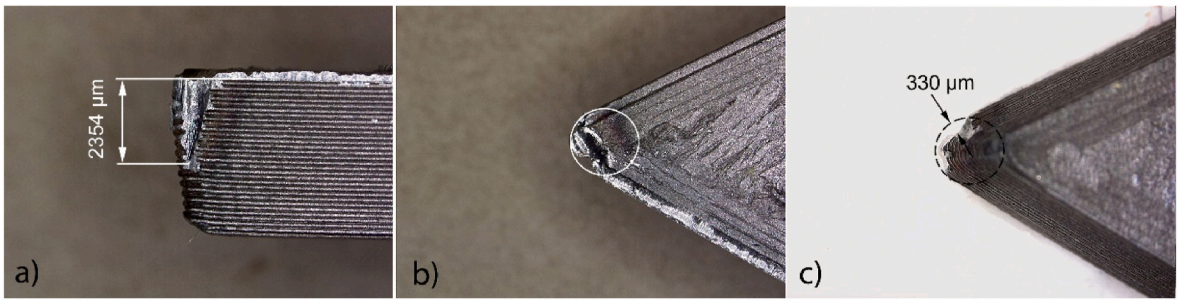

Fig. 15. Appearance of the cutting edge at the end of run E9: a) side view, b) top view, d) bottom view (V_c = 220 m/min, f = 0.25 mm/r, a_p = 0.9 mm, t = 547 s).

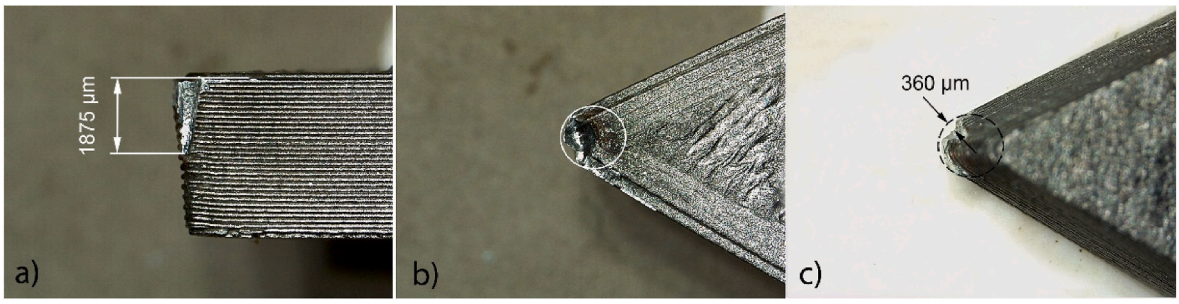

Fig. 16. Appearance of the cutting edge at the end of run E6: a) side view, b) top view, d) bottom view (V_c = 200 m/min, f = 0.25 mm/r, a_p = 0.6 mm, t = 811 s).

Furthermore, it has been verified how in experiments E9, E8, E7 and even E6, both notch wear parameters HB_N and VB_N grow exponentially, and practically before reaching 50% of the time spent performing the roughing cycle. Thus, Figs. 15 and 16 show the noticeably affected appearance of the main cutting edge at the end of experiments E9 and E6, respectively. Consequently, these specific results represent the most unfavorable working conditions for the manufactured insert since the cutting edge deteriorates quickly.

Definitely, and based on the results obtained, it seems that the most appropriate conditions for machining this type of alloy with the additively manufactured insert should be close to the technological values established in experiments E3 (light green) and E5 (light blue). Finally, and based on this technological analysis of the results we can establish, 160 m/min $\leq V_c \leq$ 200 m/min, 0.20 mm/r $\leq f \leq$ 0.25 mm/r and a_p = 1.2 mm as optimal working conditions for the insert manufactured by AM.

Focusing on the evidence of the previous analysis and stablishing the maximum wear limits ($HB_{N\ max}$, $VB_{N\ max}$) as shown in Figs. 11 and 14, it can be seen, once again, that run tests E3 and E5 define the optimal working conditions for the tool object of study. It is observed that even though the machining of the planned full volume had been achieved in a time of less than 900 s (15 min), the limit in the wear parameters had not yet been reached (see light green and light blue curves in Figs. 11 and 14). This tells us that, under these working conditions, it is possible to eliminate even more volume of material until the established edge life is consumed. Thus, for experiment E3, the working time could be increased to practically t = 600 s, this represents 61 s more time that corresponds to a possible increase of 11.3% in volume removal. On the other hand, in the conditions of experiment E5, the work could continue until t ≈ 640 s, that is, 83 s more, which represents a possible increase of 14.9% in the volume removed.

It seems that the built-in edge phenomenon has not had a significant effect on cutting edge wear, since a non-cumulative contribution of material has been observed. This fact is corroborated by observing that the aluminum added to the cutting edge is gently adhered to it and, in most cases, it is removed relatively easily from the cutting edge as it is not strongly welded. Besides, a very contained progression has been observed in the value of the height of the built-in edge (H_{BUE}) during the partial measurements carried out in all the run tests of this final experimental round, as can be seen in Tables S1–S9 of the supplementary material. Additionally, observing the values of the accumulated H_{BUE} in Tables 10 and it seems that a higher value of a_p = 1.2 mm favours the value of the built-up edge to be smaller at the end of the working cycle.

3.3. Metallographic analysis

The metallographic structure of the cutting edge of some of the most representative inserts from the test program has been analyzed. Micrographs have been obtained from an unused insert and two others subjected to severe machining conditions, E3 and E5. The results are shown in Fig. 17, which is attached.

The study reveals that inserts subjected to higher cutting speeds (Vc = 200 m/min) and greater cutting depths (a_p = 1.2 mm) caused a slight refinement in grain size in the area adjacent to the cutting edge. This could be due to localized thermal shock during the working process, as well as the pressure exerted on the surface of the turned part, effects that may have improved performance of the inserts in the case of experiments E3 and E5. According to a previous work consulted [35], an increase in hardness due to the combined effects of temperature and pressure during the work with tooling made with this type of steel has been documented. Additionally, the evident original porosity of the additively manufactured inserts could improve the effect of the cooling fluid during turning process, which likely extends the tool's service life by reducing the temperature in the cutting zone.

3.4. Statistical analysis on the influence of cutting parameters

This section presents the statistical analysis of the results obtained. To this end, the effect of the input variables (V_c, f and a_p) on each of the output variables (VB_N and HB_N) of the process has been studied through analysis of variance (ANOVA) applied to linear regression fits, in all the cases. In addition, the influence of these three input variables on the lifetime of the cutting edge of the insert was also analyzed.

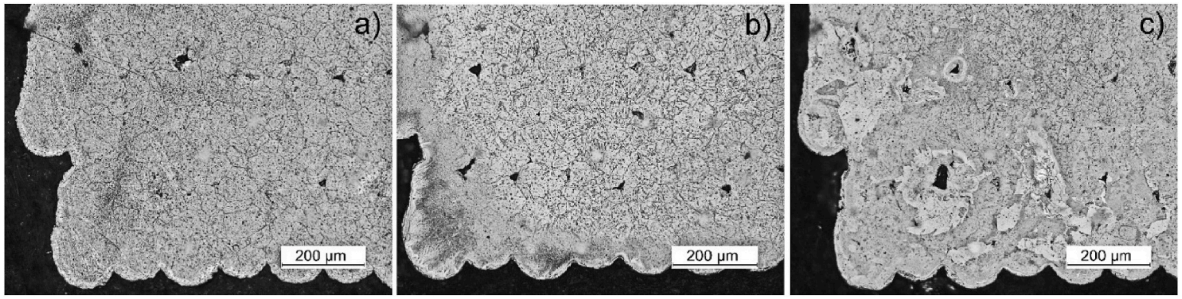

Fig. 17. Micrograph of the cutting edge of the inserts: a) not used, b) E1, V_c = 160 m/min, f = 0.15 mm/r, a_p = 0.6 mm, c) E5, V_c = 200 m/min, f = 0.20 mm/r, a_p = 1.2 mm.

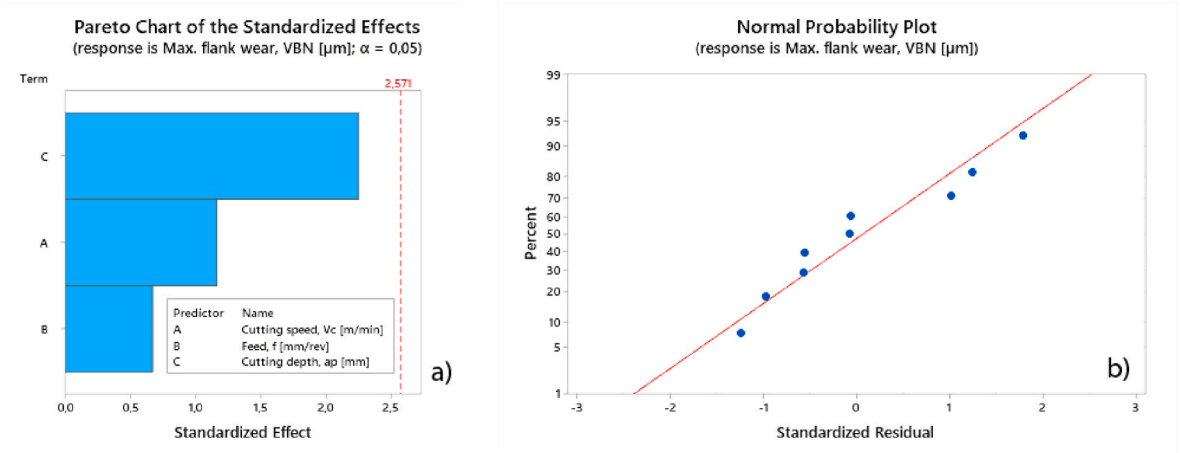

Fig. 18. a) Pareto chart of main effects and b) normal probability plot for notch wear height response, VB_N.

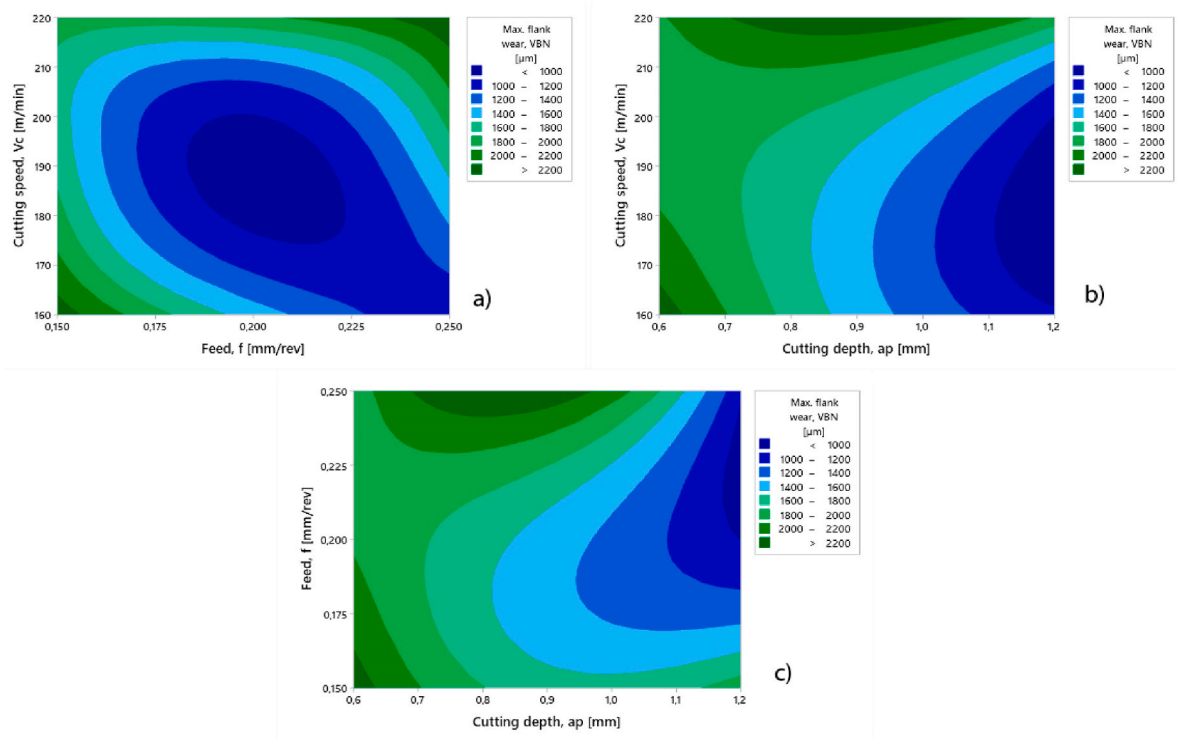

Fig. 19. Contour plots for wear relative to maximum notch height, VB_N. Combined effects of a) V_c with f, b) V_c with a_p and c) f with a_p.

3.4.1. Analysis of variance (ANOVA) of the height in the flank notch wear, VB_N

Although the R^2 value that we obtain for this regression model is too low ($R^2 = 57.91\%$), the normal probability line (Fig. 18b) certifies its validity for the ANOVA. On the other hand, the Pareto diagram (Fig. 18a) shows the variable pass depth (a_p) as the one that most affects the notch height wear (VB_N). Fig. 19 shows contour plots that relate the effect of each pair of variables on VB_N.

In the contour plots of Fig. 19b and c, when high pass depths (a_p) are combined, generally with low cutting speeds (V_c) or high feedrates (f), the height measured in the notch wear (VB_N) is minimized. Furthermore, the least wear VB_N occurs when combining intermediate feedrates around $f \approx 0.20$ mm/r with intermediate cutting speeds around $V_c \approx 180 \div 200$ m/min. Furthermore, contour plot of Fig. 18a shows that medium-high values of feedrate (f) implies the lower VBN flank wear when combined with medium-low cutting speed (V_c).

3.4.2. Analysis of variance (ANOVA) of the depth in the flank notch wear, HB_N

In this case, the linear fit presents a statistic $R^2 = 83.97\%$ which, like the distribution of the data on the normal probability graph presented in Fig. 20b, indicates that the generated model is suitable for ANOVA. Thus, the Pareto chart in Fig. 20a shows the factor pass depth (a_p) again as the most influential in the depth measured in notch wear (HB_N), followed by the cutting speed (V_c). Furthermore, this wear output is very sensitive to changes in these two input variables, while the feedrate (f) is practically does not affect. On the other hand, Fig. 21 shows the paired effect in contour plots.

Contour plots shown in Figs. 21b and c again corroborate the effect of pass depth (a_p) on wear. Thus, larger pass depths (a_p) imply less wear on the cutting edge, while cutting speeds (V_c) that are too high are not good. In this sense, the ideal way to obtain less wear is to combine values of $a_p = 0.9 \div 1.2$ mm at cutting speeds $V_c = 160 \div 200$ m/min. On the other

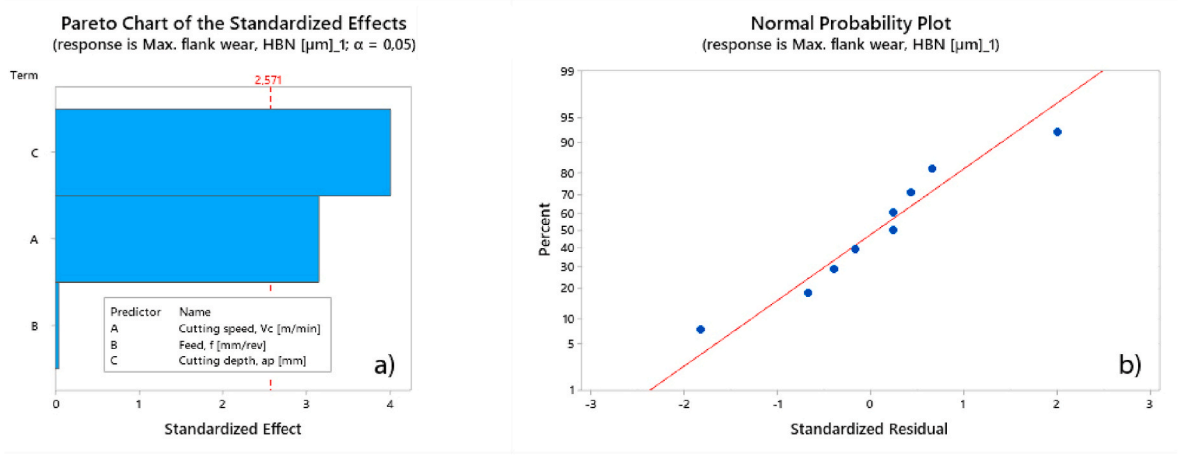

Fig. 20. a) Pareto chart of main effects and b) normal probability plot for notch wear depth response, HB_N.

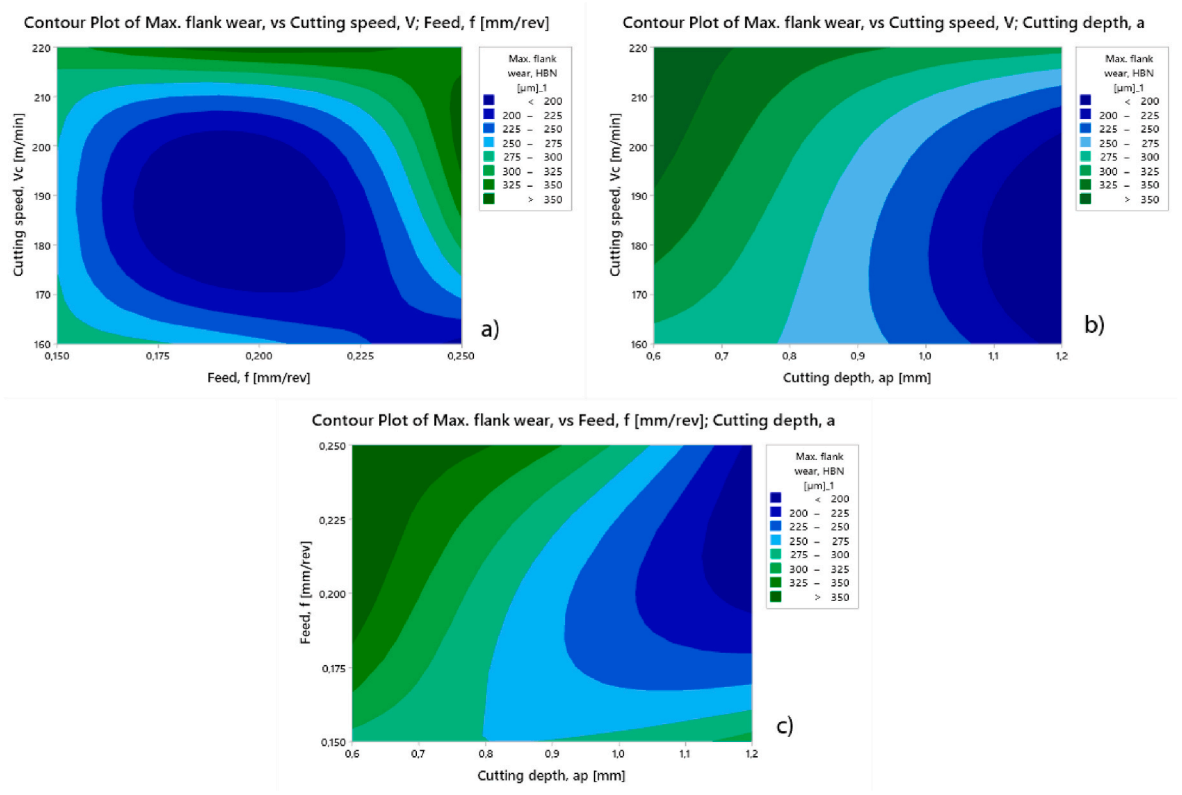

Fig. 21. Contour plots for wear relative to maximum notch depth, HB_N. Combined effects of a) V_c with f, b) V_c with a_p and c) f with a_p.

hand, in the contour graph of Fig. 21a it is observed that the ideal feedrate (f) to minimize this wear would be between $f = 0.175$ mm/r and $f = 0.225$ mm/r.

3.4.3. Analysis of variance (ANOVA) of the cycle time response

In this case, a linear regression fit was applied with $R^2 = 91.89\%$, which gives high reliability to this model. Thus, the Pareto chart in Fig. 22 indicates that the factor pass depth (a_p) is once again the one that most affects the time (t) necessary to eliminate all the material programmed in the roughing/finishing cycle, followed by the feedrate (f) and lastly the cutting speed (V_c).

Contour plots b) and c) in Fig. 23 show that the ideal a_p values to achieve a higher material removal rate are those above $a_p > 0.9$ mm, especially when combined with higher cutting speeds (V_c). However, a cutting speed range between $V_c = 160 \div 200$ m/min is also efficient when working with feedrate values $f > 0.18$ mm/r, as shown in contour plot of Fig. 23a.

Observing the results corresponding to experiments E3 ($V_c = 160$ m/min, $f = 0.25$ mm/r and $a_p = 1.2$ mm) and E5 ($V_c = 200$ m/min, $f = 0.20$ mm/r and $a_p = 1.2$ mm), it can be stated that these working conditions have allowed to obtain very balanced values between the evaluated wear parameters (HB_N and VB_N) and the cycle time (t) required for the complete roughing/finishing operation. Thus, the ideal working conditions for the manufactured insert will be around the conditions implemented in these two tests.

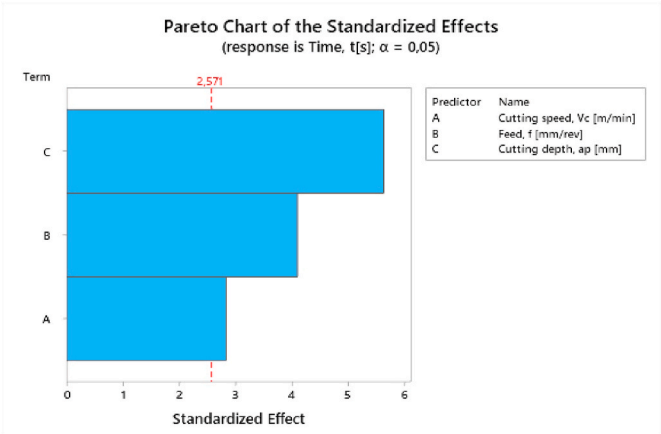

Fig. 22. Pareto chart of main effects for the cycle time response (t).

4. Conclusions

The manufacture of standardized inserts has been carried out using the Metal X additive manufacturing equipment, from the Markforged company, using a filament based on AISI H13 steel powder with polymeric binder. The inserts were subjected to various experimental tests following an orthogonal L9 arrangement designed by the Taguchi method. The experiments have been organized in four preliminary L9 sets to determine the sensitivity of cutting-edge wear versus the technological variables studied (input factors), and a final test to evaluate the useful life of the tool for a roughing/finishing cycle on EN AW-2030 aluminum specimens. Subsequently, an ANOVA was carried out on the influence of machining parameters on tool wear and cycle time.

The results show that the insert can work with cutting speeds (V_c) between 40 and 260 m/min, feedrates (f) between 0.05 and 0.25 mm/r and pass depths (a_p) from 0.1 to 2.4 mm. However, the optimal technological conditions, with wear limits $HB_{N\ max} = 250$ μm and $VB_{N\ max} = 1500$ μm, have been 160 m/min $\leq V_c \leq$ 200 m/min, 0.20 mm/r $\leq f \leq$ 0.25 mm/r and $a_p = 1.2$ mm. Furthermore, the influence of cutting speed (V_c) was examined, through ANOVA analysis revealing that tool wear is not very sensitive to its variation up to values of $V_c = 210$ m/min. In this analysis, it was determined that the feedrate (f) minimizes wear when working in a range between $f = 0.15$–0.25 mm/r, while the depth of pass (a_p) was revealed as the most influential parameter on wear, with less wear when $a_p > 0.9$ mm and offering better results when these values approach $a_p = 1.2$ mm.

The surface finish, analyzed through the mean roughness Ra, showed a high dependence on the depth of the pass, improving for low values of a_p and for relatively high cutting speeds (V_c). Regarding the feedrate (f), the roughness decreased with low values, as is known for turning.

This analysis has not only established an efficient procedure for the additive manufacturing of cutting inserts but has also demonstrated that the inserts obtained using material extrusion technique could enable machining conditions for aluminum alloys in the range of values like those recommended for commercial inserts made of tungsten carbide.

This work represents an advance in the design and manufacture of cutting inserts for turning through additive manufacturing, especially in specialized applications, by offering customized designs that are not offered in a catalog of conventional commercial inserts. The ability to build complex geometries and the possibility of creating customized designs allows a rapid solution in prototyping, repairs, or in-situ unit manufacturing, offering adaptability according to changing and specific engineering demands. These advantages, combined with the positive results obtained in the performance of the manufactured inserts, underline the relevance and transformative potential of additive manufacturing in the field of cutting tool design and materials.

Funding

This research received no external funding.

Declaration of competing interest

The authors declare that they have no known competing financial

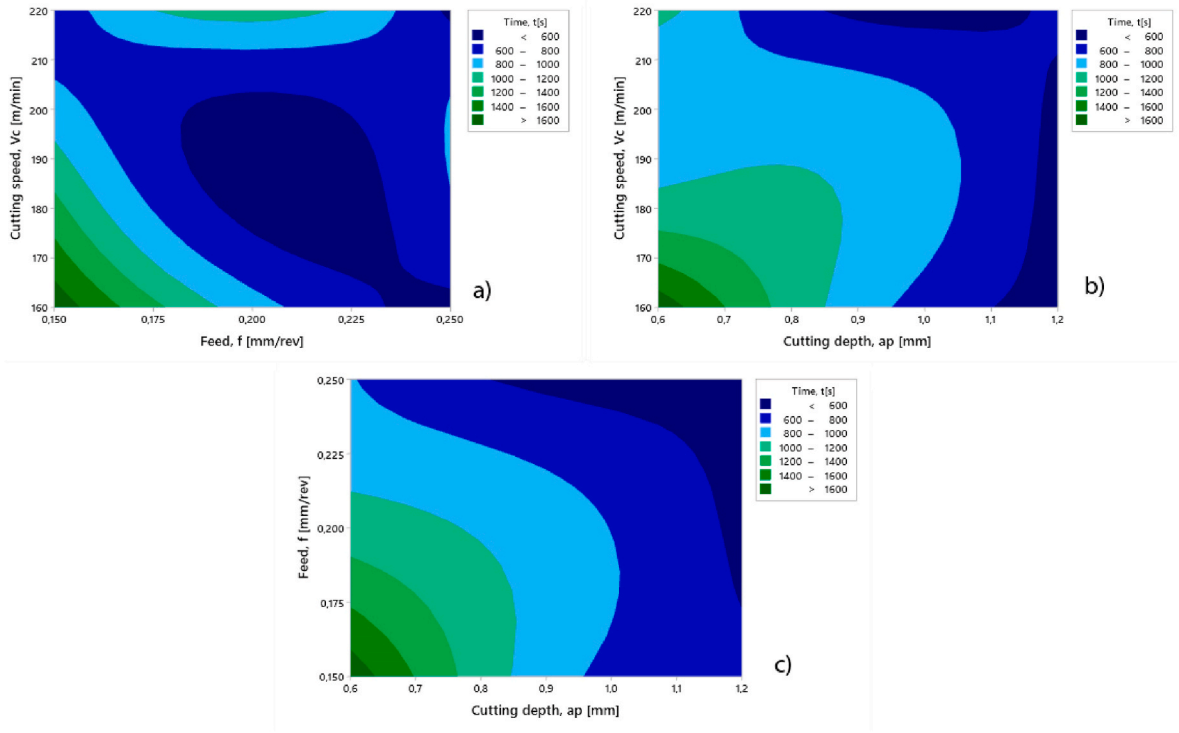

Fig. 23. Contour plots for cycle time or lifetime (t), HB_N and combined effects of a) V_c with f, b) V_c with a_p and c) f with a_p.

interests or personal relationships that could have appeared to influence the work reported in this paper.

Acknowledgements

We appreciate the work of the mechanical engineer Salvador Moreno and the laboratory technician Manuel Latorre in the execution of the experiments and the acquisition of images, respectively. We also would want to thank Dr. Francisco Comino, from the Materials Science area of the University of Córdoba, for his work in the preparation and analysis of the metallographic samples.

Appendix A. Supplementary data

Supplementary data to this article can be found online at https://doi.org/10.1016/j.jmrt.2024.05.065.

References

[1] Wang B. The Future of manufacturing: a new perspective. Engineering 2018;4:722–8. https://doi.org/10.1016/j.eng.2018.07.020.
[2] Khalilpourazari S, Khalilpourazary S, Özyüksel Çiftçioğlu A, Weber GW. Designing energy-efficient high-precision multi-pass turning processes via robust optimization and artificial intelligence. J Intell Manuf 2021;32:1621–47. https://doi.org/10.1007/s10845-020-01648-0.
[3] Colantonio L, Equeter L, Dehombreux P, Ducobu F. A systematic literature review of cutting tool wear monitoring in turning by using artificial intelligence techniques. Machines 2021;9:351. https://doi.org/10.3390/machines9120351.
[4] Abu-Mahfouz I, Rahman AE, Banerjee A. Surface roughness prediction in turning using three artificial intelligence techniques; A comparative study. Procedia Comput Sci 2018;140:258–67. https://doi.org/10.1016/j.procs.2018.10.322.
[5] Ganeshkumar S, Singh BK, Suresh Kumar R, Haldorai A. Digital twin framework for lathe tool condition monitoring in machining of aluminium 5052. Defence Sci J 2023;73:341–50. https://doi.org/10.14429/dsj.73.18650.
[6] Rall K, Loker D, Nikhare CP. Optimal machine learning for detecting lathe machining parameters. Int J Adv Manuf Technol 2023;128:779–88. https://doi.org/10.1007/s00170-023-11939-4.
[7] Asif M, Shen H, Zhou C, Guo Y, Yuan Y, Shao P, et al. Recent trends, developments, and emerging technologies towards sustainable intelligent machining: a critical review, perspectives and future directions. Sustainability 2023;15:8298. https://doi.org/10.3390/su15108298.
[8] Sykora J, Sedlmajer M, Schubert T, Merkel M, Kroft L, Kucerova L, et al. Additive manufacturing of WC-Co specimens with internal channels. Materials 2023;16. https://doi.org/10.3390/ma16113907.
[9] Xing Y, Luo C, Zhu M, Zhao Y, Ehmann K, Wu Z, et al. Assessment of self-lubricating coated cutting tools fabricated by laser additive manufacturing technology for friction-reduction. J Mater Process Technol 2023;318. https://doi.org/10.1016/j.jmatprotec.2023.118010.
[10] Sykora J, Kroft L. Additively manufacturing an indexable insert. IOP Conf Ser Mater Sci Eng 2021;1190:012025. https://doi.org/10.1088/1757-899x/1190/1/012025.
[11] Traxel KD, Bandyopadhyay A. First demonstration of additive manufacturing of cutting tools using directed energy deposition system: Stellite™-based cutting tools. Addit Manuf 2019;25:460–8. https://doi.org/10.1016/j.addma.2018.11.019.
[12] Yang Y, Zhang C, Wang D, Nie L, Wellmann D, Tian Y. Additive manufacturing of WC-Co hardmetals: a review. Int J Adv Manuf Technol 2020;108:1653–73. https://doi.org/10.1007/s00170-020-05389-5.
[13] Traxel KD, Bandyopadhyay A. Diamond-reinforced cutting tools using laser-based additive manufacturing. Addit Manuf 2021;37:101602. https://doi.org/10.1016/j.addma.2020.101602.
[14] Vafadar A, Guzzomi F, Rassau A, Hayward K. Advances in metal additive manufacturing: a review of common processes, industrial applications, and current challenges. Appl Sci 2021;11:1213. https://doi.org/10.3390/app11031213.
[15] ASTM International. A 681 – 08: standard specification for tool steels alloy. 2022.
[16] Cruz FR, Alves N, Vieira T. Direct additive manufacturing as spring of new tool steels. J Mater Res Technol 2023;26:5450–61. https://doi.org/10.1016/j.jmrt.2023.08.176.
[17] Montevecchi F, Grossi N, Takagi H, Scippa A, Sasahara H, Campatelli G. Cutting forces analysis in additive manufactured AISI H13 alloy. Procedia CIRP 2016;46:476–9. https://doi.org/10.1016/j.procir.2016.04.034.
[18] Bae K, Moon H-S, Park Y, Jo I, Lee J. Influence of tempering temperature and time on microstructure and mechanical properties of additively manufactured H13 tool steel. Materials 2022;15:8329. https://doi.org/10.3390/ma15238329.
[19] Ariza-Galván E, Montealegre-Meléndez I, Pérez-Soriano EM, Neubauer E, Kitzmantel M, Arévalo C. Influence of processing conditions on the mechanical properties of 17-4PH specimens produced by additive manufacturing. Machines 2022;10. https://doi.org/10.3390/machines10110976.
[20] Zhang J, Liu Z, Xu C, Du J, Su G, Zhang P, et al. Modeling and prediction of cutting temperature in the machining of H13 hard steel of multi-layer coated cutting tools. Int J Adv Manuf Technol 2021;115:3731–9. https://doi.org/10.1007/s00170-021-07417-4.
[21] Mirabal A, Loza-Hernandez I, Clark C, Hooks DE, McBride M, Stull JA. Roughness measurements across topographically varied additively manufactured metal surfaces. Addit Manuf 2023;69:103540. https://doi.org/10.1016/j.addma.2023.103540.
[22] Li S, Deng H, Lan X, He B, Li X, Wang Z. Developing cost-effective indirect manufacturing of H13 steel from extrusion-printing to post-processing. Addit Manuf 2023;62:103384. https://doi.org/10.1016/j.addma.2022.103384.
[23] Mishra A, Gangele A. Multi-objective optimization in turning of cylindrical bars of AISI 1045 steel through Taguchi ' s method and utility concept. Int J Sci Basic Appl Res 2013;12:28–36.
[24] Abhang LB, Hameedullah M. Optimization of machining parameters in steel turning operation by Taguchi method. Procedia Eng 2012;38:40–8. https://doi.org/10.1016/j.proeng.2012.06.007.
[25] Dhawan AP, Shinde TB. Optimization of cutting parameters in rough turning using Taguchi method. Asian Rev Mech Eng 2016;5:31–41. https://doi.org/10.51983/arme-2016.5.2.2415.
[26] Akhtar MN, Sathish T, Mohanavel V, Afzal A, Arul K, Ravichandran M, et al. Optimization of process parameters in CNC turning of aluminum 7075 alloy using L27 array-based Taguchi method. Materials 2021;14:4470. https://doi.org/10.3390/ma14164470.
[27] Tsao CC. Grey–Taguchi method to optimize the milling parameters of aluminum alloy. Int J Adv Manuf Technol 2009;40:41–8. https://doi.org/10.1007/s00170-007-1314-3.
[28] International Standard Organization. ISO 1832:2017 Indexable inserts for cutting tools - designation. 2017.
[29] European Norm. EN-ISO 573-5. Aluminium and aluminium alloys - Part 3: chemical composition and form of products, vol. 22; 2023.
[30] European Norm. EN-ISO 755-1. Aluminium and aluminium alloys. Extruded rod/bar, tube and profiles - Part 1: Technical conditions for inspection and delivery 2016;60.
[31] Coldwell H, Woods R, Paul M, Koshy P, Dewes R, Aspinwall D. Rapid machining of hardened AISI H13 and D2 moulds, dies and press tools. J Mater Process Technol 2003;135:301–11. https://doi.org/10.1016/S0924-0136(02)00861-0.
[32] European Norm. EN-ISO 6508-1:2023. Metallic materials - Rockwell hardness test - Part 1 : test method 2023:39.
[33] International Standarization Organization. ISO 6983-1:2009 (E), Automation systems and integration - numerical control of machines - program format and definitions of address words - Part 1: data format for positioning, line motion and contouring control systems. Geneva: ISO; 2009.
[34] International Organization for Standardization. UNE EN ISO 21920-3:2023 Geometrical product specifications (GPS) - surface texture: profile - Part 3: specification operators. 2023.
[35] Li C, Han Y, Li E, He S, Ren J. Microstructure and microhardness of H13 and Cr8 die steels in control forging and cooling process. J Mater Eng Perform 2022;31:4983–97. https://doi.org/10.1007/s11665-021-06303-0.